QPS PROGRESS REPORT

EXECUTIVE SUMMARY

While the basic QPS configuration has not changed since the September 2000 Project meeting, there has been outstanding progress during this period in improving the QPS concept. We are on track for the early May 2002 Conceptual Design, Cost and Schedule Review (CDR) and the Project Validation Review in late May. The improvements in the plasma and coil configuration since the April 2001 QPS Physics Validation Review (PVR) have had the following consequences.

(1) Neoclassical transport losses have been reduced by a factor ~15 since the PVR reference case; they are now at the same level as in the large German Wendelstein 7-X (W 7-X) stellarator, which has 4 times the plasma aspect ratio R/a of QPS.

(2) The open space in the central coil bore has been increased to accommodate the toroidal field (TF) coil legs and Ohmic current (OH) solenoid.

(3) The plasma-coil and coil-coil spacings have been increased.

(4) The modular coils have been modified to reduce errors in reconstructing the optimized field by a factor of 2.2.

(5) The vacuum vessel has been modified to eliminate eddy currents induced by the poloidal field (PF) system.

The plasma and coil configuration is satisfactory for the more detailed study needed for the May CDR and many of the issues raised by the PVR panel have been addressed.

In addition, there have been important developments in the German Wendelstein 7-AS (W 7-AS) stellarator program since the April PVR that put QPS on a sounder basis. We had projected electron Bernstein wave (EBW) heating at high plasma density on the basis of theory and EBW *emission* measurements in tokamaks. Now W 7-AS has actually demonstrated efficient EBW *heating* at high plasma density. The second development from W 7-AS is use of a magnetic island divertor geometry (similar to that in QPS) *without* additional pumping to obtain robust operation at 4×10^{20} m^{-3} plasma density with gas fueling and to raise the volume-average beta from $\langle\beta\rangle = 1.8\%$ to $\langle\beta\rangle = 3.1\%$.

QPS PROGRESS REPORT

1. QPS Status at the April PVR

The "gb4" reference plasma configuration discussed in detail at the PVR was adequate for the QPS mission, but significant improvements were possible as evidenced by some results for an improved "gb5" configuration that was also presented at the PVR. The plasma configuration and the filamentary modular coils that create it are shown for gb4 PVR reference configuration in Fig. 1 and the improved gb5 plasma configuration is shown in Fig. 2. The colors indicate the strength of |B| in Teslas on the last closed flux surface (LCFS); |B| varies by a factor of 2.66 over the LCFS in Fig. 2. A sharp helical ridge is seen in Fig. 2 resulting from a small radius of curvature of the LCFS over a range of toroidal angles. Although the gb5 configuration had substantially improved

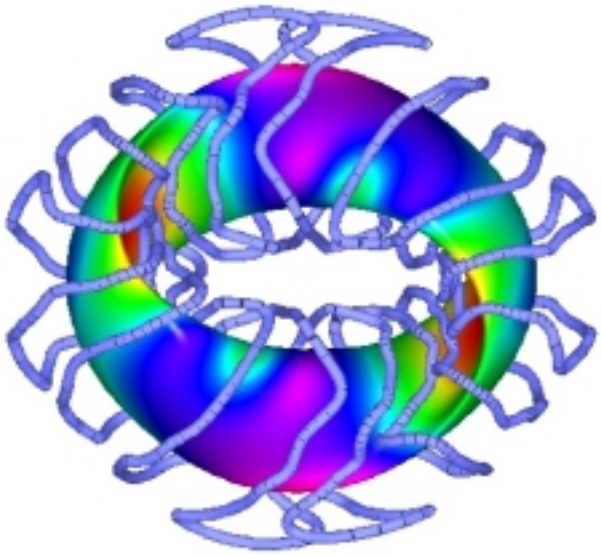

Fig. 1. The gb4 PVR reference plasma and coil configuration.

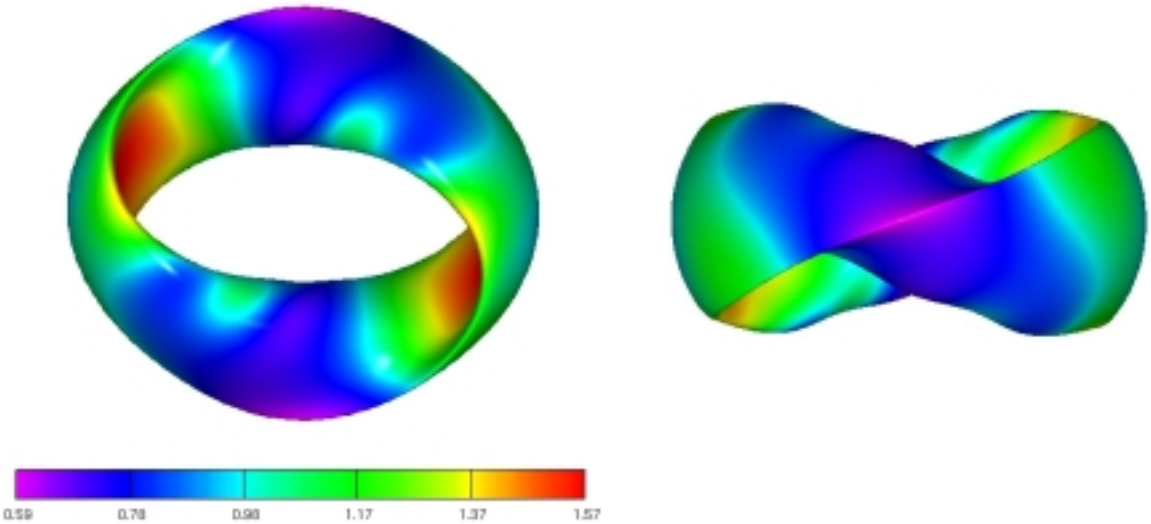

Fig. 2. Top and side view of the improved gb5 plasma configuration shown at the PVR.

neoclassical confinement, it did not have adequate space in the middle for the TF coil center legs and an OH solenoid.

A number of physics, engineering, and programmatic issues were also identified by the PVR panel that needed attention including looking for a higher-β, second stability regime. Progress in these areas is also reported here.

2. Improvements in the QPS Plasma Configuration since the PVR

Work since the April PVR has focused on both improving the neoclassical confinement even beyond that exhibited by the gb5 configuration and increasing the space in the open central bore beyond that for the more feasible gb4 coil configuration. The result is the two-field-period racetrack configuration shown in Fig. 3. It has sixteen modular coils, four of each type. The four

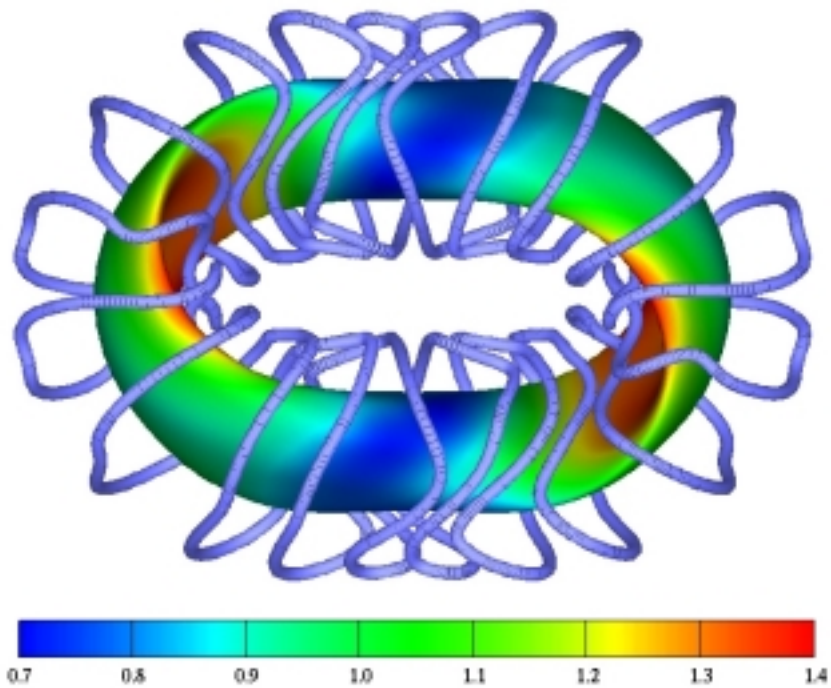

Fig. 3. Top view of the QPS plasma and coil configuration.

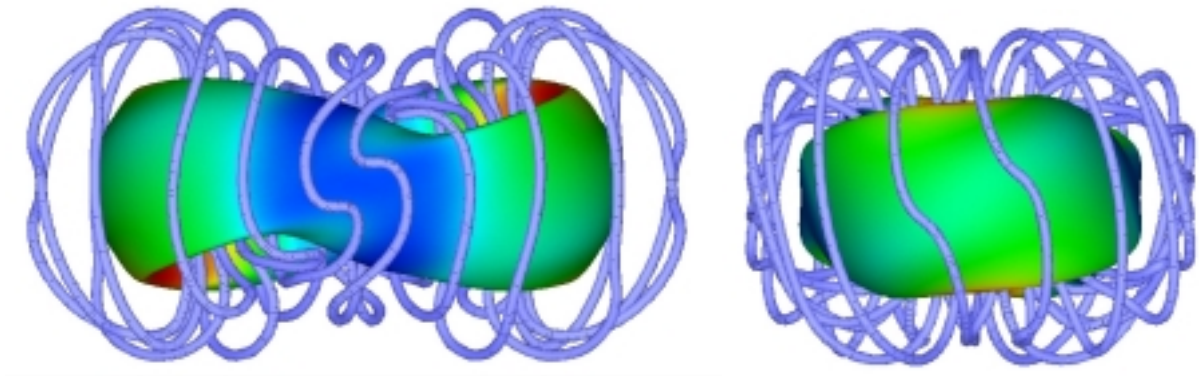

Fig. 4. Side views of the QPS plasma and coil configuration.

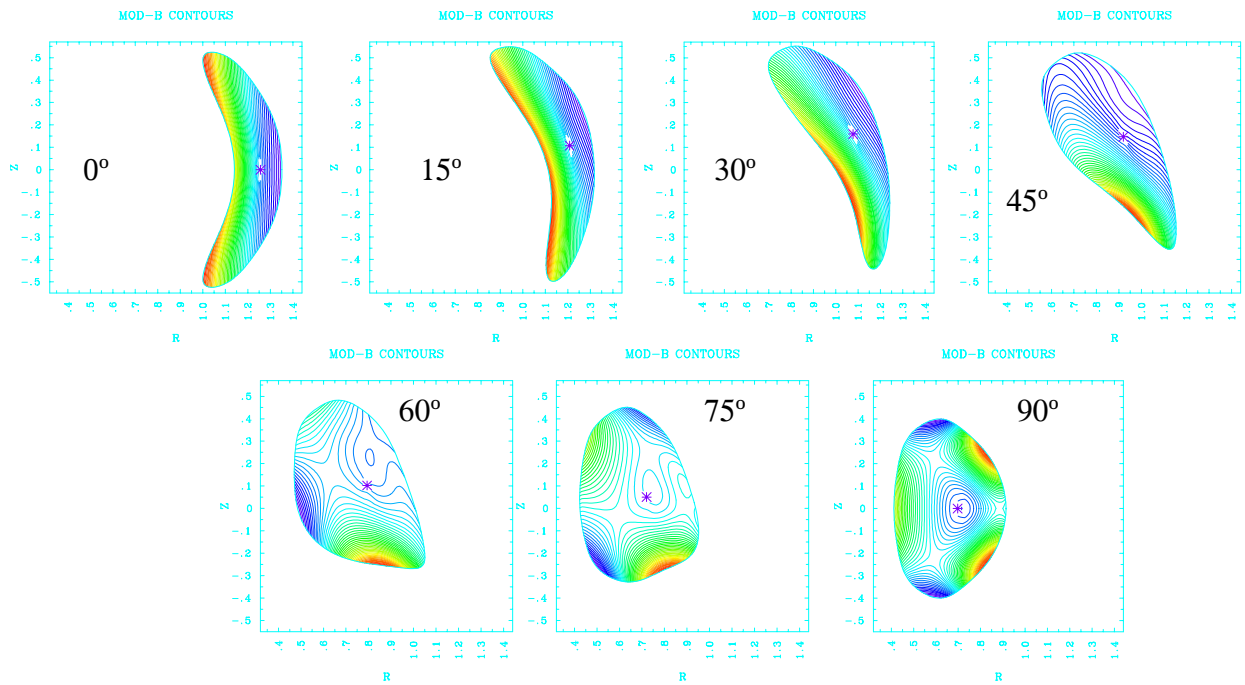

Fig. 5. Cross sections through the QPS flux surfaces at different toroidal angles showing contours of constant |B| strength.

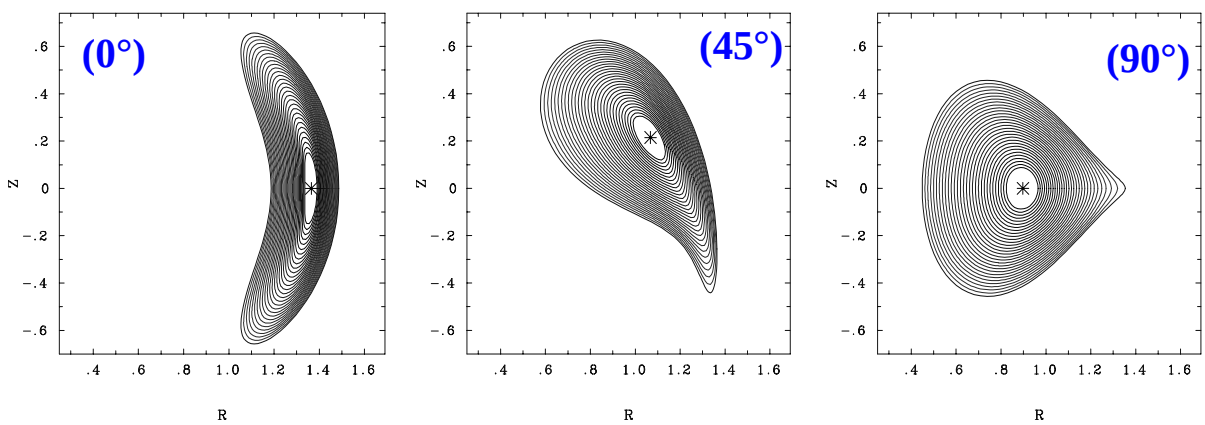

Fig. 6. Cross sections of the gb5 flux surfaces at three toroidal angles.

filamentary "coils" in the middle of the long sides are really two coils that are split. The value of |B| varies by a factor of 2 over the LCFS in Fig. 3. Side views from the middle of the long side and the end are shown in Fig. 4. The pattern of the |B| contours on the LCFS is more poloidally banded for the QPS configuration than for the PVR configuration in Fig. 1.

Figure 5 shows cross sections of the flux surfaces for a number of toroidal angles in a half field period. The colors indicate the same values of |B| as in Figs. 3 and 4 and the curves shows contours of |B|. The |B| contours are parallel (tokamak-like) for about half of each field period, and become closed (more like the flux surfaces) near the D-shaped cross section in the middle of the long side. Figure 6 shows corresponding cross sections of the flux surfaces for three of these

angles in a half field period for the gb5 configuration. The LCFS for the QPS configuration is more rounded and does not exhibit the sharp edge seen in Fig. 2.

The effective ripple ε that should be used in a single-helicity calculation of the low-collisionality 1/ν transport to give the correct neoclassical ripple-induced transport is obtained from the NEO code. Figure 7 shows $\varepsilon^{3/2}$ (proportional to the heat diffusivity) for a number of stellarators. As a result of the improvements in the QPS plasma configuration since the April PVR, the low-collisionality neoclassical transport losses have been reduced by a factor ~15 from the PVR reference configuration; the losses are now at the same level as in W 7-X, which has 4 times the *R*/*a* of QPS.

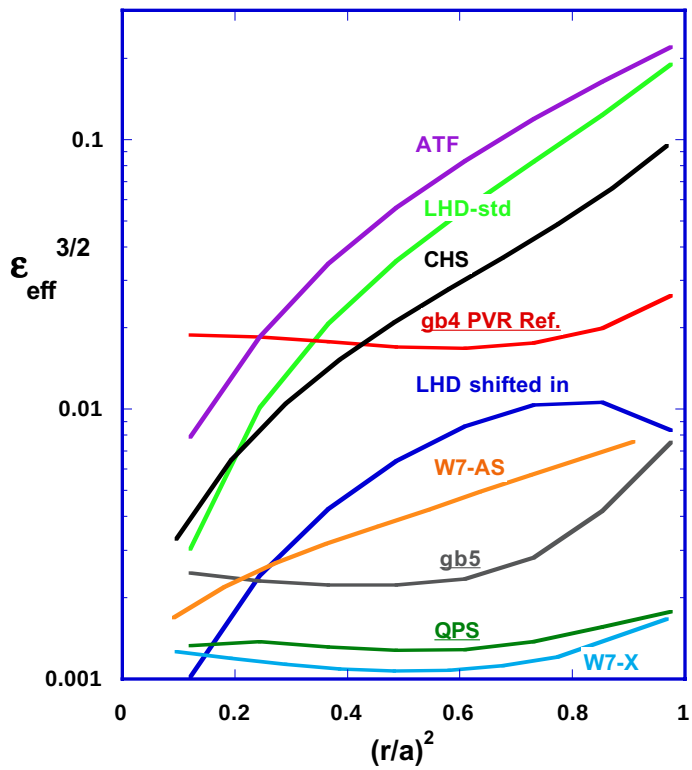

Fig. 7. Relative ripple-induced low-collisionality transport from the NEO code.

The effect of the improved neoclassical transport on the performance of QPS at low collisionality is illustrated in Fig. 8 for a 1.5-MW electron-cyclotron-heated (ECH) plasma at $n_e = 2 \times 10^{19}$ m^{-3}. The 1-D transport calculation assumes an anomalous transport corresponding to a factor of 1.5 improvement over the ISS-95 stellarator scaling (the Japanese Large Helical Device, LHD, and W 7-AS have obtained up to 2.5 times the ISS-95 confinement) and the ripple-induced neoclassical transport corresponding to the ripple in Fig. 7 in the Shaing-Houlberg model with a self-consistent ambipolar radial electric field. The ripple-induced neoclassical transport is a perturbation in the power flows at intermediate radii for the QPS configuration whereas it was the dominant component of the power flow for the reference gb4 PVR configuration. The effect on the resulting electron temperature profile is shown in Fig. 9. The large ripple-induced loss over most of the plasma interior leads to lower central electron temperature and a broader profile compared to the QPS case.

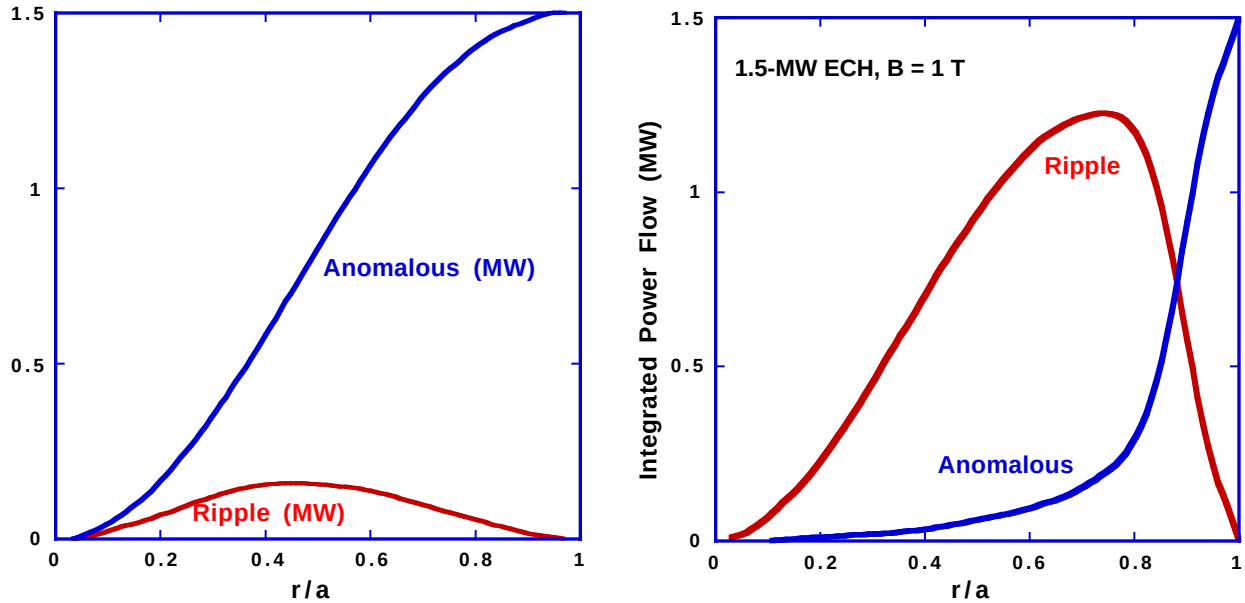

Fig. 8. Integrated power flow through r/a for QPS (left) and the gb4 PVR reference case (right).

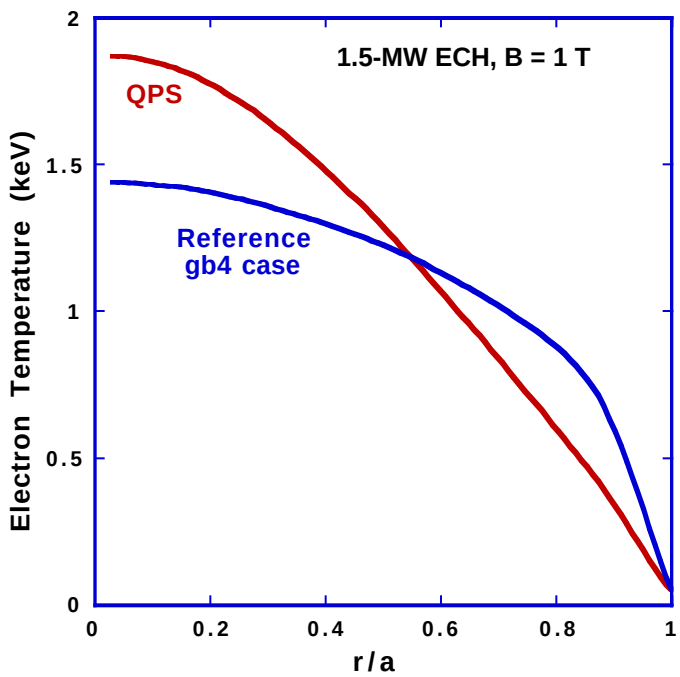

Fig. 9. Effect of increased ripple-induced transport (gb4 case) on the electron temperature profile.

3. Improvements in the QPS Design since the PVR

Excellent reconstruction of the optimized LCFS is obtained using the filamentary coils, as shown in Fig. 10. This figure shows cross sections of the LCFS at four toroidal angles for the optimized plasma configuration (dashed curves) and the LCFS obtained from the filamentary coils (solid curves). There is relatively little difference between the optimized and reconstructed LCFS.

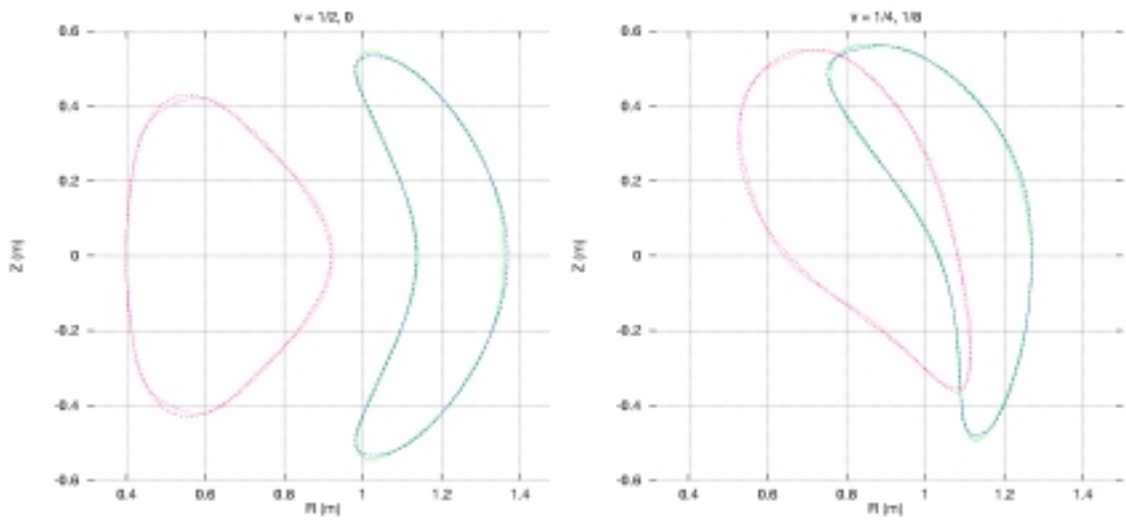

Fig. 10. Reconstruction of the optimized LCFS from the filamentary coils.

The engineering embodiment of the QPS coil configuration is shown in Fig. 11, which indicates the actual size of the coils. Each of the 16 modular coils has two rectangular conductor bundles separated by a stainless steel "T". The "T" is relatively thin for 12 of the coils, but the two conductor bundles are more widely separated in the four coils in the middle of the long legs of the racetrack configuration. This was done to reduce the errors in reconstructing the optimized field by more than a factor of two. The web between the conductor bundles in these coils can be seen better in Fig. 12, which shows a cutaway view of QPS in its bell jar vacuum tank. The open space in the central coil bore in Fig. 11 has been increased to accommodate the 12 TF coil legs and the four OH solenoid windings. The central opening is larger than that for the PVR gb4 reference configuration for added margin. The background TF field has been increased from ±0.15 T to ±0.2 T and the Ohmic current capability has been increased from ±50 kA to ±150 kA. The plasma-coil and coil-coil spacings have also been increased. The minimum distance between the LCFS and the modular coil pack is now 9 cm and the modular coils can now be oriented perpendicular to the coil winding

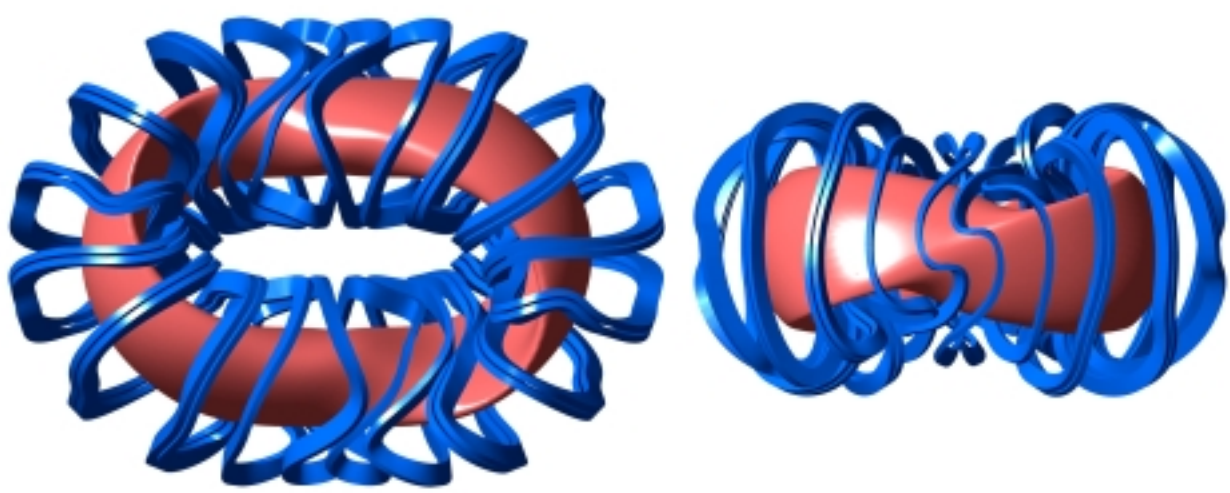

Fig. 11. QPS LCFS and modular coil configuration: top view (left) and mid-side view (right).

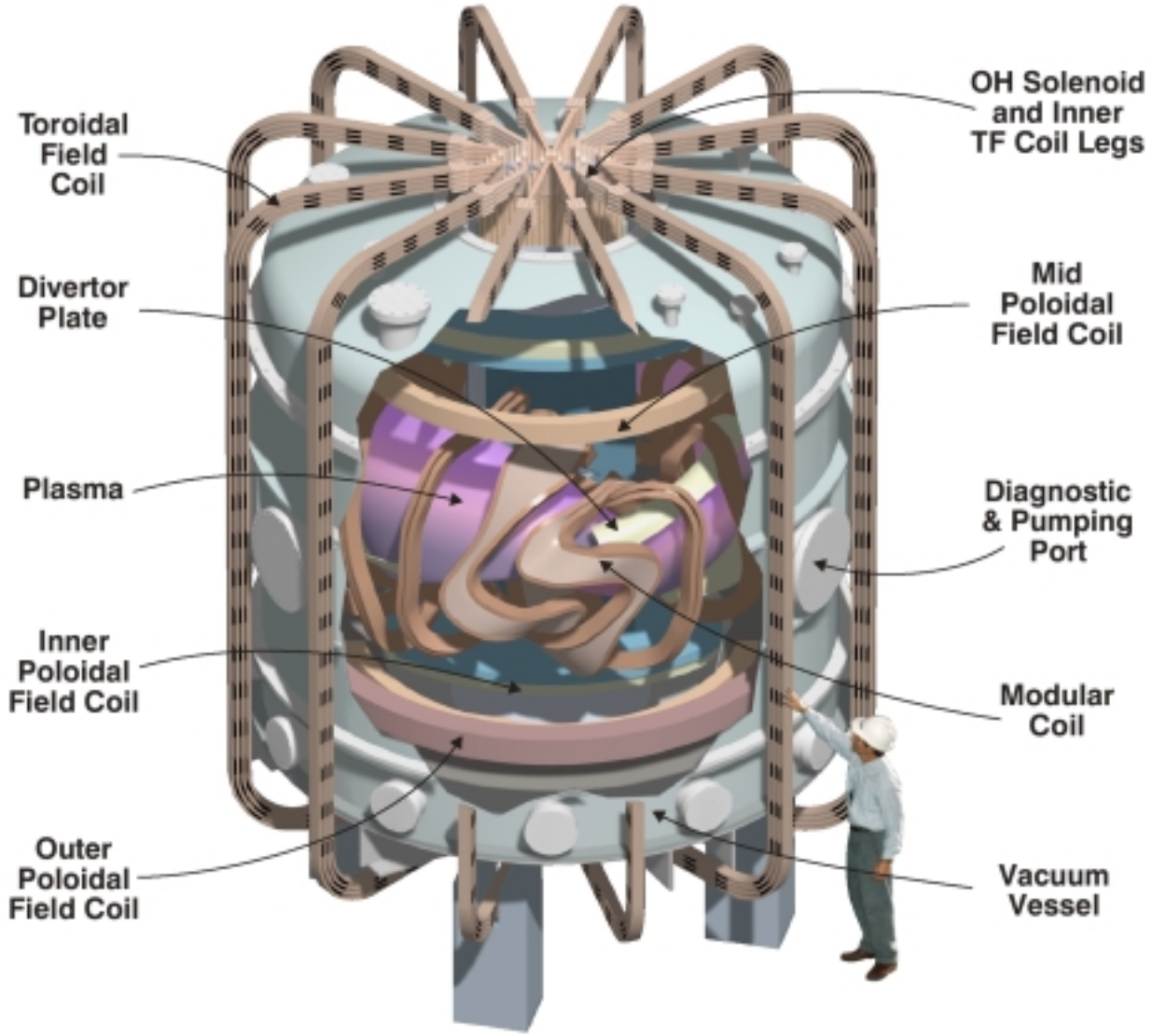

Fig. 12. Cutaway view of QPS in its bell jar vacuum tank.

surface for easier fabrication. The only remaining issue is the need to increase the bend radius of the central modular coils on the inside at the top and bottom. The smaller bend is in the plane of the coils far removed from the plasma, so it should not be difficult to remedy this.

The aluminum spool piece that formed the original cylindrical side of the ORMAK vacuum vessel has been replaced by a stainless steel spool piece. In addition to eliminating eddy currents induced by the PF system, this change: (1) allows use of metal seals, instead of differentially pumped viton seals that can outgas, to obtain lower base pressure in the vacuum tank; (2) eliminates the rectangular access door that required differentially pumped viton seals; and (3) allows twelve large (61-cm diameter) ports for diagnostic, heating, and personnel access.

4. Improved Outlook for QPS

The improved QPS configuration is the result of advances in stellarator optimization and coil design codes at ORNL. Incorporation of the NEO code (written by Kernbechler and Nemov) into the ORNL stellarator optimization code STELLOPT provided access to new QPS designs with improved neoclassical transport. In addition, work on the ORNL drift kinetic equation solver (DKES) transport code has improved its convergence, and therefore its predictive capabilities, in the low collisionality regime. Substantial progress has also been made in the development of the ORNL coil design code COILOPT. A major breakthrough in coil development for QPS (and the national compact stellarator experiment, NCSX) has recently been achieved by replacing the global Fourier expansion representation of the modular coils with a local B-spline representation. This allows greater control of local coil bend radii, which is a crucial coil engineering constraint that was previously difficult to control with the Fourier expansion method. For QPS, this spline representation has resulted in much lower magnetic field errors. This allows improved reconstructions of the plasma (from the coils) and preservation of physics properties for the very low R/a QPS configuration. Although further improvements can be expected from using the recently combined ORNL plasma optimization code STELLOPT and the COILOPT code, which bypasses the intermediate step of finding an optimized LCFS, the present QPS plasma and coil configuration is satisfactory for the more detailed study needed for the May CDR. The combined STELLOPT/COILOPT code is now being used to obtain feasible coils for NCSX and will be applied to QPS as well.

In addition, there have been important developments in the W 7-AS program since the April PVR that put QPS on an even sounder basis. We had projected EBW heating at high density on the basis of theory and EBW *emission* measurements on tokamaks. Now W 7-AS has actually demonstrated efficient EBW *heating* at high plasma density (3.5×10^{20} m^{-3}).

Another important development in the W 7-AS program is use of a magnetic island divertor geometry (similar to that in QPS) *without* additional pumping to obtain robust operation at n_e up to 4×10^{20} m^{-3} with gas fueling. Above a threshold plasma density that depends on heating power, the energy confinement time τ_E increases steeply with increasing density, and the particle confinement time τ_p and the impurity confinement time τ_{imp} both decrease with increasing plasma density. The density profile changes from peaked to flat with steep density gradients at the edge. The radiated power is peaked at the edge and quasi-steady-state operation is obtained with stationary density. The high-density divertor operation has resulted in $\langle\beta\rangle$ increasing from 1.8% to 3.1%. The plasma stability increases with increasing $\langle\beta\rangle$; the magnetohydrodynamic (MHD) activity is largest at intermediate $\langle\beta\rangle$ values and is relatively small at the highest $\langle\beta\rangle$. There is no effect of MHD activity on confinement; τ_E is still about twice the ISS-95 scaling value at the highest $\langle\beta\rangle$.

High central electron temperatures (T_{e0}), up to 7 keV, are obtained with ECH at the plasma density assumed for QPS ECH operation, $n_e = 2 \times 10^{19}$ m^{-3}. The T_e profiles are centrally peaked and exhibit an internal transport barrier due to electron-root operation, similar to that observed in the Japanese Compact Helical System (CHS) and LHD stellarators. This mode of operation would lead to higher T_e values in QPS than those projected on the basis of the assumed $1.5 \times$ ISS-95 confinement scaling.

5. Progress on the PVR Issues

Satisfactory progress is also being made on issues identified by the QPS PVR panel. The July 2001 report summarized calculations after the PVR relating to a high-β second-stability regime in QPS, requirements for high-β operation in QPS, and access for high-power neutral beam injection in QPS. Figure 13 shows the normalized ballooning growth rates ($\gamma\tau_A$) for QPS free-boundary equilibria for a range of beta values from that report. In this case the plasma is ballooning unstable (positive $\gamma\tau_A$) from $\langle\beta\rangle$ = 2.6% to $\langle\beta\rangle$ = 5.4% and stable for higher $\langle\beta\rangle$ values, indicating a second stable regime. The pressure profile for these cases was *not* optimized. These results indicate that a region of second stability may exist for the QPS coil configuration. Further calculations will be done on accessibility to the second-stability regime for the CDR report.

Table 1 gives the status of actions on comments made by the QPS PVR panel. A number of issues have already been addressed. Those that require interactions with the international stellarator community at the Canberra International Stellarator Workshop have been postponed until the rescheduled work-shop occurs (at the end of February 2002).

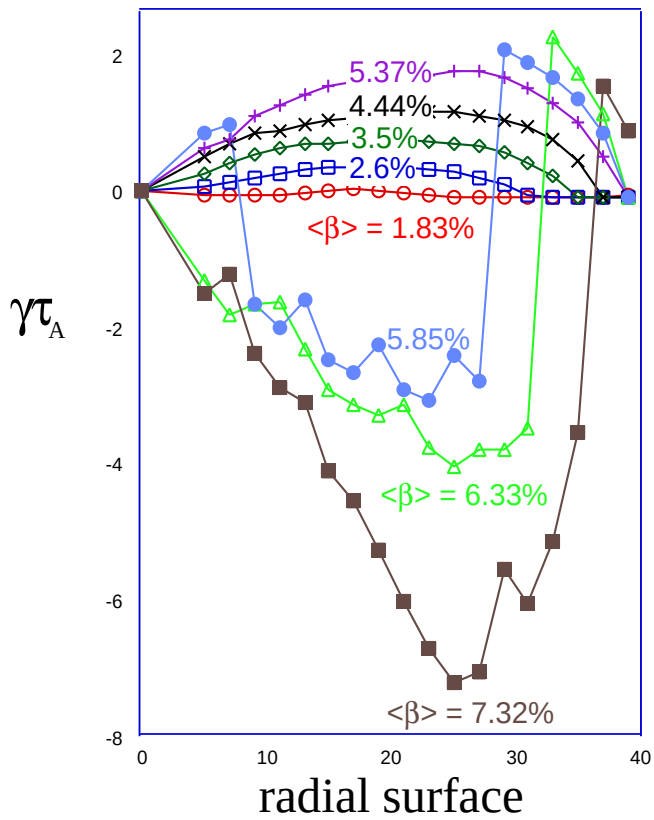

Fig. 13. Existence of a second stability regime in QPS.

6. Near-Term Work

Progress is also being made on the other issues identified by the QPS PVR panel. Most of these will be reported in the documentation for the CDR. The near-term work is focusing on issues that address the physics base for QPS. These include the following.

(1) The QPS team is refining the improved QPS configuration and improving the modular coil set that creates it and the PF coil set that allows configuration flexibility and ohmic plasma current.

(2) The Princeton PIES code will be used to examine islands at finite beta when PIES has been modified to better calculate QPS cases. Island healing studies will be continued after final optimization of the QPS modular coil set.

(3) The ORNL AVAC code will be used to assess the effects on the flux surfaces of various types of errors in coil shape or positioning. It will also be used to assess the volumes associated with magnetic islands, ergodic field regions, and well-formed surfaces for different modular and PF coil currents.

(4) We will evaluate the effects of variation of the dipole and quadrupole components of the PF on the |B| spectrum, low collisionality electron transport, and flux surface quality.

(5) 1-D calculation of temperature profiles including neoclassical ripple-induced transport with a self-consistent ambipolar electric field and ISS-95 anomalous transport will be continued to determine the profile diagnostics and modeling capability needed for unraveling the roles of neoclassical and anomalous transport.

(6) Sequences of free-boundary equilibria will be analyzed as $\langle\beta\rangle$ is increased from 0 to 2-3% for different magnetic configurations in QPS. We will continue exploring possible regimes of second stability operation in QPS.

(7) ORNL will develop a plan to team with the LHD, W 7-AS, HSX, and CTH groups to establish ICRF operation at high density.

(8) We will continue discussions with various university groups to firm up interest in collaboration on QPS.

Table 1. Status of QPS PVR Disposition Plan

Item	PVR Panel Comment or Concern	Status
Flux Surfaces Quality		
II-A1	The committee encourages recent improvements in the coils/configurations and directions to pursue before a design freeze is required.	A much improved plasma configuration with a more practical coil set has been found, as described in this report.
II-A4	Some measure other than qualitative visual examination of flux surface plots should be developed.	The AVAC code can be used to assess the volumes associated with magnetic islands, ergodic field regions, and well-formed surfaces for any coil set.
Confinement Issues		
II-B2	Adequate profile diagnostics and modeling capability should be available for unraveling the roles of neoclassical and anomalous transport.	1-D calculation of temperature profiles including neoclassical ripple-induced transport with a self-consistent ambipolar electric field and ISS-95 anomalous transport shows an easily measurable change in the shape of the temperature profile for larger ripple.
Vacuum Issues		
II-C1	More detailed interaction with operating devices dealing with problem of achieving good vacuum conditions and maintaining plasma cleanliness.	Discussions have been held with the MAST group on in-vessel components and vacuum issues and a meeting has been arranged with the H-1 group.
II-C2	Neutral penetration may be a problem and should be examined for both high and low density regimes.	Discussion with the W7-AS and CHS groups indicate that this will not be a significant issue for QPS because of its larger size compared to those experiments.
II-C3	Baking internal components to as high a temperature as feasible is encouraged.	Discussions have started with an epoxy supplier (CTD) on the highest operating temperature consistent with a feasible potting procedure. The epoxy and baking temperature will be chosen in Jan. 2002.
II-C4	Although polymer seals can work reasonably well, consider hard seals wherever possible.	Metal seals will be used on all ports on the bell jar except for the large seals on the spool piece (to reduce costs).
II-C5	Reconsider use of ORMAK vessel because of concern about aluminum center ring.	The aluminum part of the bell jar will be replaced with a stainless steel spool piece.
Diagnostics		
II-E1	Attention must be paid to good diagnostic access early in the design process (e.g., in determining apertures in the vacuum vessel).	A first cut at port allocation has been made. 12 ports 61 cm in diameter maximize the access to the plasma for diagnostics and heating.
II-E4	There should be preparation, both theoretical and in diagnostic development, to implement equilibrium and profile reconstruction from experimental data.	An ORNL/GA proposal for development of 3-D equilibrium reconstruction from experimental data based on the 3-D VMEC code and the EFIT experience is being funded.